CrossMark

ORIGINAL ARTICLE

Effect of upstream flow regime on street canyon flow mean turbulence statistics

Karin Blackman · Laurent Perret · Eric Savory

Abstract The effect on the flow over a street canyon (lateral length/height, L/h = 30) of using either 3D (cube) or 2D (rectangular block) upstream roughness arrays, of the same height as the canyon, has been studied for two streamwise canyon width to height aspect ratios (AR = W/h) of 1 and 3, in a wind tunnel using Particle Image Velocimetry. The mean streamwise velocity, shear stress, turbulent intensities and length scales, together with shear layer boundaries and mass fluxes across the canyon opening are presented for different combinations of skimming and wake-interference regimes using different upstream roughness and canyon configurations. These results show significant trends with canyon aspect ratio and roughness array plan area packing density (λ_p) with respect to 2D and 3D configurations. The mean streamwise velocity for configurations of equal λ_p is higher in 3D than 2D configurations, while the spatially averaged shear stress is shown to be lower in 3D than 2D configurations. The relative contribution to the total turbulent kinetic energy (TKE) demonstrates that staggered and aligned arrays or 2D and 3D arrays do not produce similar profiles of TKE. Finally, the integral length scale is larger in 2D cases than 3D cases of equal λ_p. Urban air quality is a significant concern for human health. By investigating the influence of upstream roughness on canyon flow one can determine which cases or flow regimes in both the upstream roughness and canyon will result in decreased ventilation and negatively effect the air quality of urban areas. From the present work decreased ventilation occurs in the skimming flow regime and is lowest in the case of upstream 2D bar roughness with $\lambda_p = 50$ % and canyon AR = 1.

Keywords Boundary layer · Street canyon · Particle Image Velocimetry · Wind tunnel

K. Blackman (✉) · E. Savory
University of Western Ontario, London, ON, Canada
e-mail: kblackm2@uwo.ca

E. Savory
e-mail: esavory@uwo.ca

L. Perret
Ecole Centrale de Nantes, LUNAM Université, Nantes Cedex 3, France
e-mail: laurent.perret@ec-nantes.fr

1 Introduction

A simple street canyon model reproduces the main features of most common street configurations, specifically for the case for which the upstream wind is perpendicular to the street axis. When modeling this configuration in the wind tunnel, Savory et al. [33] have noted, firstly, it is crucial to match the non-dimensional parameters of roughness length z_o/h, (where z_o is the aerodynamic roughness length and h is the height of the canyon) and integral length scale (L_u/h), within a factor of 2–3, between the model and full-scale to ensure the terrain type is essentially equal in both cases. Secondly, the geometry of the roughness used to generate the boundary layer is important as 2D block arrays enforce 2D behaviour of the large coherent structures generated whereas 3D arrangements reproduce more closely the 3D turbulent structure of the atmospheric boundary layer (ABL). Finally, comparison between different wind tunnel experiments of the same configuration can only be made quantitatively for those cases where the normalized displacement height (d/h) is approximately the same. These observations demonstrate the importance of aerodynamic scaling when modeling street canyons and the sensitivity of the canyon flow to the approaching boundary conditions, characterized, in particular, by z_o. Besides aerodynamic parameters such z_o/h and d/h, two other important parameters emerge from the literature: the aspect ratio $AR = W/h$ (where W is the canyon streamwise width) of the studied street canyon and the roughness plan area density (defined as the ratio of the plan area of the roughness elements to the total plan area $\lambda_p = A_p/A_d$) of the roughness array over which the flow develops. The steady flow regimes of street canyons, with varying aspect ratio AR, have been well studied, including; "skimming", "wake interference" and "isolated roughness" [24], classified by Grimmond and Oke [7] and Macdonald et al. [20] both as a function of W/h and also in terms of z_o/h, d/h and λ_p.

Although λ_p has been shown by Grimmond and Oke [7] to have a significant impact on the flow within a canyon, it is postulated here that the roughness geometry (two or three dimensional (2D or 3D) elements) employed to generate the flow in which the studied canyon is immersed also has an important effect. The present study is a comparative analysis of aerodynamically scaled boundary layers with modified upstream configurations, including both 3D and 2D roughness elements, and their effect on the flow in 2D canyons of different aspect ratio. The roughness plan area density λ_p and AR are modified for the upstream roughness and for the canyon, respectively, to include both skimming and wake interference regimes. The following review concerns experimental studies except where stated otherwise. Issues with aerodynamic scaling in previous studies are well documented by Savory et al. [33] and are, therefore, not discussed here.

The mean flow of street canyons in roughness arrays can be defined based on vertical profiles of horizontal streamwise averages of mean velocity, turbulence statistics, integral length scales and mass flux all spatially averaged across the canyon opening. Very few studies have examined the effect of varying the geometry (2D or 3D) of the roughness elements on the boundary layer flow, and it is difficult to compare them as the nature of the roughness differs for each study (see list of previous studies and their configurations in Table 1). The configurations used in these studies provide limited information, as they do not use multiple configurations with varying λ_p for each type of roughness, 3D or 2D. In their study of the pollutant removal from a street canyon of $AR = 1$, Michioka and Sato [23] did study two geometries, both within the skimming flow regime. When using the mean velocity at $z = 2h$, they found that the Reynolds shear stress increases from 2D to 3D configurations, as does the friction velocity. This change of geometry has a small effect on the mean velocity profiles within the canopy. Similarly, the friction velocity and shear stress (normalized by the freestream velocity) were found to increase from 2D to 3D

Table 1 Summary of parameters for canyon and roughness array investigation

Reference	Method	2D or 3D	Array*	λ_p (%)	Canyon AR	U_e (m/s)	u_* (m/s)	Compared in figures
Barlow and Leitl [1]	Exp.	2D	–	63, 50	–	6	0.44, 0.44	
Cheng et al. [3]	Exp.	3D	A	6.25, 25	–	10	0.65, 0.68	z_o, $<\overline{u'w'}>$
			S	6.25, 25	–		0.73.0.71	
Coceal et al. [4]	DNS	3D	S	25	–	–	–	–
Hagishima et al. [8]	Exp.	3D	A	25	–	8	–	z_o
			S	25	–		–	
Ho and Liu [9]	Exp.	2D	–	50, 3, 25, 11, 9, 8	–	2.5	–	ACH
Huq and Franzese [10]	Exp.	3D	A	13, 25, 19	–	0.078, 0.094, 0.11	-	$\overline{U}$, σ_u
Kanda et al. [13]	LES	3D	A	0, 44	–	1	–	z_o
Kanda [14]	LES	3D	S	0, 44	–	1	–	–
Lee et al. [16]	Exp.	3D	S	4	–	–	–	L_u
		2D	–	11	–	–	–	
Lee et al. [17]		2D		25				
	DNS	3D		12.5	–	–	–	–
Liu et al. [18]	LES	2D	-	66, 50, 33	–	–	–	
Macdonald [19] and Macdonald et al. [20,21]	Exp.	3D	A	5, 33	–	1.5	0.2, 0.24	z_o
			S	5, 33	–		0.22, 0.24	
Marciotto and Fisch [22]	Exp.	2D	–	11, 14, 20	–	10	0.62, 0.62, 0.81	–
Michioka and Sato [23]	LES	3D	A	25	1	1	0.099	
		2D	–	50, 33	1		0.067, 0.092	
Rafailidis [27]	Exp.	2D	–	66, 50	–	5	–	σ_u
Ricciardelli and Polimeno [28]	Exp.	3D	A	36	–	10	–	–
Rivet [29]	Exp.	3D	S	25	–	5.9	0.38	$<\overline{U}>$, σ_u, $<\overline{u'w'}>$, $\overline{U}$
Salizzoni et al. [31]	Exp.	2D	–	25, 33, 40, 50	1	6.75	0.46, 0.41, 0.36, 0.33	$\overline{U}$, σ_u
Sato et al. [32]	Exp.	3D	A	11, 25, 44	1	0.65	0.065	$\overline{U}$, σ_u
Savory et al. [33]	Exp.	3D	S	6.25	–	5.9	0.345	z_o, $\overline{U}$, σ_u

Table 1 continued

Reference	Method	2D or 3D	Array*	λ_p	Canyon AR	U_e (m/s)	u_* (m/s)	Compared in figures
Takimoto et al. [34]	Exp.	3D	A	44, 25, 18	–	2	0.22, 0.27, 0.27	$<\overline{U}>$, L_u, $<\overline{u'w'}>$
		2D	–	50	–		0.15	
Volino et al. [35]	Exp.	3D	A	–	–	1.247	0.0603	L_u
		2D	–	11	–	0.5	0.0341	

*A aligned, S staggered

configurations throughout the boundary layer by Volino et al. [35]. Lee et al. [17] found a similar trend when the streamwise spacing of roughness elements was smaller than 5h but the opposite when the spacing increases. No clear information about the influence of λ_p was given. The influence of varying the roughness geometry on the turbulence integral length scales was also investigated. Volino et al. [35] and Lee et al. [16,17] found that this change of geometry has a strong influence, with larger length scales above the roughness for 2D cases than 3D cases [35], but Takimoto et al. [34] show no consistent variation of integral length scales between the 2D and 3D cases. Of the studies presented here, Volino et al. [35] makes the most definitive conclusions concerning integral length scales. However, those conclusions are founded upon a limited number of configurations, only one 2D and 3D case, with the 3D case consisting of a rectangular mesh formed from circular section elements compared to the 2D square bars. Other researchers have studied only 2D or 3D arrays, with the work tending to focus on the effect of roughness aspect ratio or plan area density.

2D roughness can also be used to represent a street canyon and using this configuration reproduces the important flow mechanisms, such as turbulent organized structures, sweeps and ejections and a separated shear layer, while *a priori* reducing complexity [26]. Here, those papers that have used 2D square bar roughness to represent street canyons and those that have used them simply for roughness arrays are examined. Each of the following cases used roughness elements and canyons of equal height. The turbulent eddies defined by integral length scales within the skimming flow regime were found to be limited or suppressed within and above the roughness by the large λ_p [9,31]. This is further confirmed by Rafailidis [27] who noted that λ_p within the skimming flow regime has only a mild effect on the turbulence statistics at z/h = 1 and above. On the contrary, the turbulence is increased at z/h = 1 by the flow impinging on the windward face in the isolated roughness regime [9]. Salizzoni et al. [31] also noted that in the wake interference regime the turbulent structures and turbulence intensity are larger than in the skimming flow regime above the roughness. The shear stress was found to vary with λ_p within and above the roughness up to a height of approximately 5h [31]. When investigating the shear layer size no significant difference was found between the skimming and wake interference regimes. Finally, for all cases they found that the dynamics of the shear layer and the flow, characterized by the r.m.s. of the streamwise and vertical velocity fluctuations, within the cavity is significantly influenced by the turbulent kinetic energy (TKE) in the external flow.

Arrays of 3D roughness elements have been used to reproduce the three-dimensionality of the turbulence near the ground within the atmospheric boundary layer. The height below which the boundary layer is influenced by the roughness was found to be approximately

4h by Cheng et al. [3]. This is slightly higher than the value of 3h found for a 2D case in skimming flow [27]. The spatially averaged vertical profiles of streamwise velocity do not differ significantly between aligned and staggered configurations [19]. The effect of alignment (staggered or aligned) on the spatially averaged turbulent shear stress near the ground for all λ_p, as well as above the roughness for low λ_p, is significant, as found by Cheng et al. [3]. Huq and Franzese [10] determined that near the ground this stress is comparable for all aligned cases tested of varying λ_p. As well, Cheng et al. [3] showed that the shear stress is dependent on λ_p for aligned cases and not significantly dependent for staggered cases above the roughness height and within the shear layer. However, it was determined that the relationship between λ_p and turbulence statistics is insignificant for aligned arrays above the roughness, but significant within the roughness [13]. Salizzoni et al. [31] determined that the shear stress is dependent on λ_p, whereas Marciotto and Fisch, who also studied 2D arrays [22], found it is not. Of the studies including aligned arrays some determined that shear stress is not dependent [10] on λ_p while others found it was [3]. There is much inconsistency in regard to the relationship between shear stress and λ_p, therefore no definite conclusion can be drawn from the available studies. Through quadrant analysis at z/h = 1 Kanda et al. [14] suggest that the ventilation determined by quadrant analysis of aligned arrays is sensitive to λ_p, whereas it is not for staggered arrays. Finally, z_o is shown to be higher for staggered arrays than aligned cases for all λ_p [8,20]. Grimmond and Oke [7] do not distinguish between aligned and staggered 3D arrays in their study of the effects on z_o of λ_p. In both 2D and 3D cases it is shown that the vertical profiles of streamwise velocity increase in magnitude with increasing λ_p [13,31].

From the above review several conclusions can be drawn with respect to the differences between 2D and 3D configurations from studies using only 2D configurations or only 3D configurations. The spatially averaged shear stress is higher above the roughness in the 3D case, but configuration type has negligible impact within the roughness [3,23]. Studies of turbulence intensity show contradictory results as it is larger above the roughness in 2D than 3D configurations when comparing the results of some studies [10,27], but it is also noted to be similar above the roughness when comparing others [10,31]. A similar discrepancy is apparent in the vertical profiles of streamwise mean velocity with 2D cases having higher values than 3D cases [4,31] or *vice versa* [10,31].

Ho and Liu [9] and Liu et al. [18] include analysis of the mass flux or air exchange rate (ACH) which is based on the time-averaged flow rate across the 2D canyon opening and can be separated into the mean, turbulent and total components, which can be used as a measurement of the ventilation rate. Both studies determined that the mass flux increases with decreasing λ_p [9,18]. Ho and Liu [9] also found that the turbulent fluctuations dominate the total mass flux for all cases tested. Liu et al. [18] compared very dense arrays ($\lambda_p = 67, 50$ %) with a slightly less dense array ($\lambda_p = 33$ %) and found that the former cases had approximately equal mass flux, but the latter case had greater mass flux than that of the other two cases by a factor of 2 as it falls within the wake interference regime compared to the other skimming flow regime cases.

The interaction between the boundary layer over roughness arrays with different λ_p and canyons with different AR has not been previously studied extensively through experiments in the same facility and with a comprehensive range of configurations. In particular, the role of the effect of turbulence generated locally and in the oncoming boundary layer upon the flow in the canyon and its ventilation characteristics remain unclear. Recently, Marciotto and Fisch [22] investigated a 2D canyon with varying AR = 4, 6, and 8 and, surprisingly, concluded that "the flow within the canyon is little sensitive to the turbulence level of the flow above" a statement which is claimed to be supported by Ricciardelli and Polimeno [28], but is

contradicted by Salizzoni et al. [31] who found that the structure of the external flow influences the structure of the cavity flow. Although Ricciardelli and Polimeno [28] noted that the mean and fluctuating characteristics of canyon flow are more dependent on local geometry than that of the oncoming flow, that observation was made on the basis of measurements within large obstacles in only two boundary layers, one with a smooth ground plane and one with very small roughness elements when compared with the measurement roughness obstacles. This meant that not only were the oncoming flows insufficiently turbulent, but their study did not cover a wide enough range of configurations to provide sufficient evidence for such a claim. Ricciardelli and Polimeno [28] also state that the turbulence within the canyon seems to be "a superposition of the oncoming large-scale turbulence and of the locally generated small-scale turbulence". However, previous evidence has shown that there is coupling rather than merely "superposition", between the local and oncoming turbulent flow characteristics [2,8,15,26,31].

From this present overview it may be seen that many studies have investigated roughness arrays through a variety of methods. Discrepancies are apparent when comparing 2D and 3D cases of equal λ_p using statistics such as turbulence intensity, integral length scale, streamwise velocity, and Reynolds shear stress. The spatially averaged turbulent shear stress for staggered arrays has been shown to be insensitive to λ_p above the roughness, while the shear stress of aligned arrays has been shown to be sensitive to λ_p above the roughness, but not within. Additionally, z_o is shown to be higher for staggered than aligned 3D arrays. However, each of these studies lack a significant range of configurations, including both 2D and 3D arrays falling within both the skimming flow regime and the wake interference regime, to determine the effects of upstream roughness on the canyon flow. Furthermore, several of the studies have not used proper aerodynamic scaling for them to simulate realistic urban arrays or street canyons. From this review several questions still remain:

- What is the impact of using aligned versus staggered arrays on the turbulent statistics within and above the canyon?
- What is the effect of using 2D versus 3D obstacle arrays on the turbulent statistics within the canyon, the shear layer and the overlying boundary layer?
- What is the effect of λ_p on the turbulent statistics throughout the boundary layer within both the skimming flow regime and the wake interference regime?

The overall goal of the present research is to determine the oncoming boundary layer mean flow and turbulence statistics and those of street canyons for realistic scales and a range of configurations in order to; (a) determine the differences between the boundary layer produced by 2D and 3D obstacle arrays with equal λ_p and their interaction with canyons of AR representing two different regimes (skimming and wake interference) according to the Oke [24] categorization and (b) to investigate the dynamics of the flow and structure of the turbulence. This paper focuses on part (a).
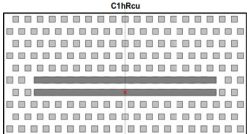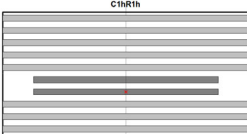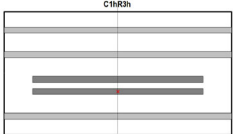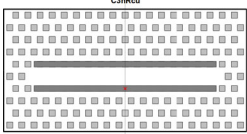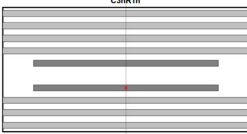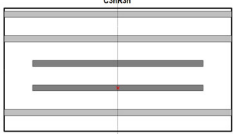
2 Experimental details

The experiments were conducted in the low-speed, suck-down boundary layer wind tunnel in the LHEEA at Ecole Centrale de Nantes (Fig. 1), which has working section dimensions of 2 m (width) × 2 m (height) × 24 m length and a 5:1 ratio inlet contraction. The empty-tunnel has a free-stream turbulence intensity of 0.5 % over a wind speed range of 3–10 m/s with good spanwise uniformity to within ±5 % [33]. The experiments used five 800 mm high vertical tapered spires located immediately downstream of the contraction and a 200 mm
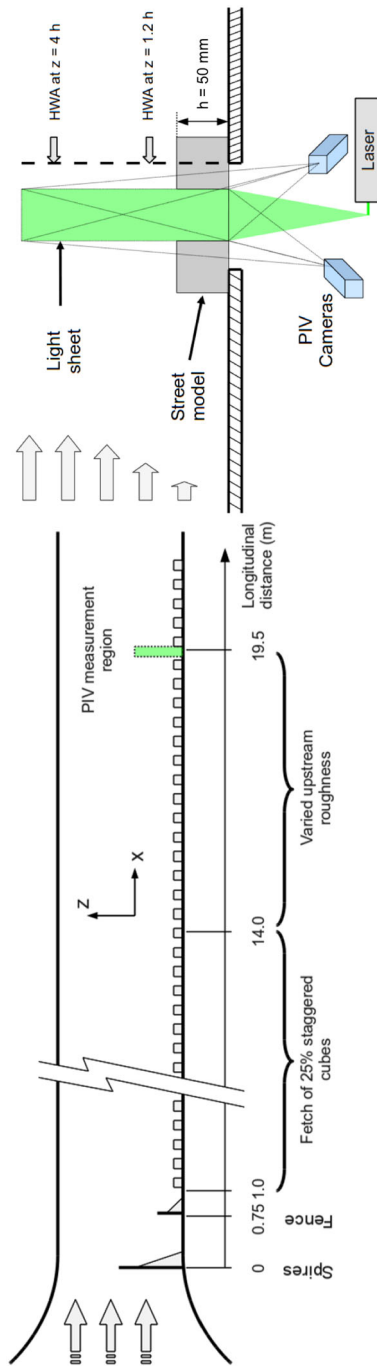
Fig. 1 *Left* wind tunnel set-up; *right* stereoscopic PIV set-up

Table 2 Canyon configurations studied in the present work

Roughness	25% Staggered cubes (Rcu) $\lambda_p = 25\%$	2D bars, spacing: 1h (R1h) $\lambda_p = 50\%$	2D bars, spacing: 3h (R3h) $\lambda_p = 25\%$
Canyon width			
W = 1h (C1h)	C1hRcu	C1hR1h	C1hR3h
W = 3h (C3h)	C3hRcu	C3hR1h	C3hR3h

high solid fence across the working section 750 mm downstream of the spires to initiate the boundary layer development. These were followed by an initial 13 m fetch of 50 mm staggered cube roughness elements with a plan area density of 25 % to initiate boundary layer development. The canyon flow measurement tests were taken 5.5 m downstream of this initial development region whilst the roughness arrays over this last portion of the wind tunnel floor were either 50 mm cubes arranged in a staggered array with $\lambda_p = 25$ % or 50 mm square section, two-dimensional bars that spanned the width of the tunnel, with an element spacing of either 1 or 3 h. Six flow configurations were investigated: two canyon widths of W/h = 1 or 3, with 3 different types of upstream roughness elements (Table 2). The measurement canyons are defined as Cnh with n = 1 or 3, and the upstream roughness (Rm) is staggered cubes (m = cu) or 2D bars with m = 1 or 3 h. The canyon building length was L = 30 h, with the canyon height h = 50 mm.

The velocity fields were measured in a vertical plane in the centre of the canyon aligned with the free stream flow direction (Fig. 1, right). A Dantec particle image velocimetry (PIV) system set up in stereoscopic configuration and located beneath the wind tunnel floor was used to measure the three velocity components. A commercially available smoke generator was used to seed the flow with water-glycol droplets of a diameter with distribution mean of 1 μm. To ensure proper seeding of the lower part of the boundary layer the seeding particles were introduced just downstream of the contraction section of the wind tunnel. The particles were illuminated for PIV measurement using a light sheet generated by a Litron double cavity Nd-YAG laser (2×200 mJ). A frequency of 7 Hz was used between pairs of pulses and two CCD cameras with a 60 mm objective lens were used to record pairs of images. A time-step of 400 μs was set between two images of the same pair. The synchronization of the cameras and laser was controlled using Dantec Dynamic Studio software, which was also used to perform the PIV analysis of the recorded images. 5000 pairs of images were recorded for each flow configuration and the multi-pass cross-correlation PIV processing resulted in a final interrogation window size of 16×16 pixels with an overlap of 50 %. For all the configurations, the final spatial resolution was 0.83 and 1.68 mm in the longitudinal and vertical directions, respectively. In addition, two single hot-wire anemometer probes (HWA) were used to measure the streamwise velocity component above the downstream canyon block at heights of 1.2 and 4 h (Fig. 1, right). These measurements, synchronized with the PIV system to allow for accurate correlation, were performed with a sampling rate of 10 kHz. The maximum standard deviation of the main PIV statistics due to statistical

error were estimated by making the assumptions that the velocity distributions are Gaussian and were found to be of 0.0041, 0.0029 and 0.0002 for the mean velocity, velocity standard deviation and turbulent shear stress normalized by freestream velocity, respectively. The error of repeatability of the experiments can be estimated by comparing the flow statistics obtained for the same upstream roughness elements and different canyon width in the upper region where the canyon geometry influence is expected to be negligible. This error was found to be smaller than that due to the statistical convergence. All the experiments were performed with the same free-stream velocity $U_e = 5.9$ m s^{-1} measured with a pitot-static tube located at x = 15 m, y = 0 m and z = 1.5 m, giving a Reynolds number, based on canyon height, of $Re_h = 1.9 \times 10^4$.

The spanwise homogeneity was investigated by Rivet [29] over the cube array (Rcu) for z/h > 2. It was determined that the turbulence statistics taken at three spanwise measurement locations were in agreement, to within 5 % [29]. In addition, Savory et al. [33] showed that the centre-line mean flow profiles were independent of canyon length when L/h > 9 and the canyon length in the present work (L/h = 30) greatly exceeds that value.

By employing an initial $x_{tr} = 13$ m fetch of staggered cubes, the experimental setup used in the present work leads to a change in terrain for both the R1h and R3h configurations. This, in turn, leads to the development of an internal boundary layer (IBL) which forms downstream of the roughness transition. The goal in the present work is not to investigate in detail the effect of the surface change on the flow evolution but, rather, to characterize the basic properties of the flow in the measurement section (x = 19.5 m) as well as to ensure that the flow has reached equilibrium state, at least in the lowest part of the boundary layer. For more details on flow over changing terrain, the reader is referred to Chap. 4 of Kaimal and Finnigan [12]. Previous studies have shown that a discontinuity of surface roughness is always accompanied by a change in surface momentum flux, which affects the characteristics of both the mean velocity profile and the turbulence [12]. This terrain transition can be primarily characterized by the parameter $M = \log(z_{01}/z_{02})$ where z_{01} and z_{02} are the roughness lengths upstream and downstream of the roughness discontinuity, respectively. Based on the use of the parameter M, analytical models have been developed to describe the longitudinal evolution downstream of the transition of both the depth of the IBL (δ_{IBL}) and the ratio of surface stresses τ_{01}/τ_{02} [12]. In the present work, the model of Panofsky and Dutton [25] is employed to estimate the depth of the IBL as a function of the longitudinal distance x − x_{tr} after the transition, where $\kappa = 0.4$ is the Von Karman constant and B_1 is a constant equal to 1.25 [12] (Eq. 1).

$$\frac{\delta_{IBL}}{(x - x_{tr})}\left[\log\left(\frac{\delta_{IBL}}{z_{02}}\right) - 1\right] = B_1\kappa \tag{1}$$

The evolution of τ_{01}/τ_{02} is estimated using the model proposed by Jensen [11] that gives a direct estimation of the stress ratio as a function of the local IBL depth (Eq. 2).

$$\frac{\tau_{02}}{\tau_{01}} = \left[1 - \frac{M}{\log(\delta_i/z_{02})}\right]^2 \tag{2}$$

The results of these two models are shown in Fig. 2 for both the R1h and R3h configurations, where z_{01} corresponds to the roughness length of the flow developing over the cube array (Rcu) and z_{02} corresponds to the roughness length of the flow developing over either the R1h or the R3h configuration (see Sect. 3.2.1 and Table 3 for a complete description of the characteristics of the flows). The terrain transition leads to the development of an IBL, the depth of which extends beyond the PIV measurement area (Fig. 2a). The largest IBL was obtained for the R3h configuration, which has the largest roughness length and corresponds
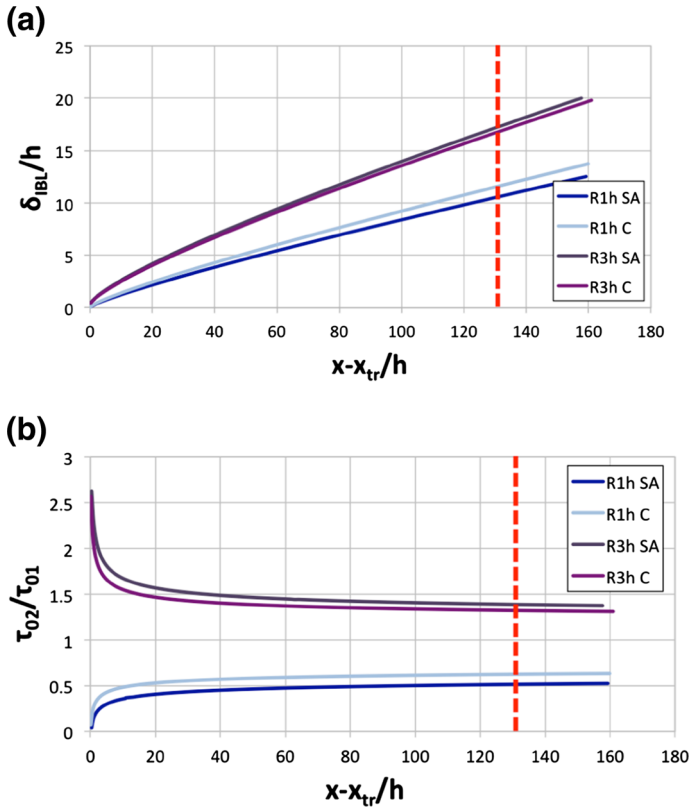
Fig. 2 Estimated development of **a** the depth of the IBL [25] and **b** the shear stress [11] downstream of the terrain change with measurement location (*red dashed lines*), where SA = using spatially averaged and C = using centre profiles

Table 3 Boundary layer characteristics, where SA and C denote the values derived from spatially averaged and centre vertical velocity profiles, respectively

Roughness	Profile	u_*/U_e	d/h	z_o/h
Staggered cubes (Rcu)	SA	0.066	0.892	0.061
$\lambda_p = 25\%$	C	0.064	0.900	0.060
2D bars, 1h spacing (R1h)	SA	0.047	0.980	0.008
$\lambda_p = 50\ \%$	C	0.049	0.927	0.015
2D bars, 3h spacing (R3h)	SA	0.072	0.552	0.143
$\lambda_p = 25\ \%$	C	0.070	0.725	0.125
$\lambda_p = 25\ \%$ [7]	–		0.600	0.120
$\lambda_p = 50\ \%$ [7]	–		0.800	0.080

to smooth to rough transition. As expected, the terrain discontinuity induces an overshoot in surface stress and the attainment of a new equilibrium as the flow adjusts to the new terrain (Fig. 2b). After a distance of 40h, it can be considered that an equilibrium state has been

reached. It is noticeable that, despite its simplicity, the prediction of τ_{01}/τ_{02} of the model proposed by Jensen [11] at the most downstream location (corresponding to the PIV measurement section) agrees very well with the value of the surface stress obtained directly from the estimation of the friction velocity based on the use of the shear stress profile, for both configurations. Hence, from these results it may be considered that, for the 3 configurations, the fetch is sufficient for the flow to reach an equilibrium state at the measurement section (x = 19.5 m). In the same manner, the estimated longitudinal integral length scales of the flow (Fig. 4d) are noticeably smaller than the distance from the terrain transition, which confirms that the investigated canyon flows are free from the initial transition influence.

In the present work the turbulence quantities are defined as follows. The instantaneous velocity components in the x, y and z directions are streamwise (U), spanwise (V) and vertical (W), respectively. Ensemble averages are denoted as $\bar{x}$ with spatial averaging denoted by $< x >$. Using Reynolds decomposition the mean velocity is $U(t) = \overline{U} + u'(t)$, where $\overline{U}$ is the time averaged velocity and $u'(t)$ is the instantaneous turbulent velocity. The standard deviation of the velocity is $\sigma_u = \sqrt{\overline{(U(t) - \overline{U})^2}}$ with the turbulence intensity, $I_u, = \sigma_u/U$. The shear stress is $\overline{u'w'} = \sqrt{\overline{(U(t) - \overline{U})} * \overline{(W(t) - \overline{W})}}$. Finally, the 3D turbulent kinetic energy is $TKE = 0.5^* \left(\sigma_u^2 + \sigma_v^2 + \sigma_w^2\right)$.

3 Results and discussion

The following section will first describe the scaling of the three approaching boundary layers considered in the present work to determine what full-scale cases are being represented. This is followed by an investigation of the approaching boundary layers to determine the influence of packing density λ_p and array obstacle configuration on the mean turbulence statistics including a comparison with literature. Finally, the role of the canyon AR will be investigated using all six configurations from the present work along with those from the literature.

3.1 Scaling of the approaching boundary layers

The PIV profiles taken at x = 19.5 m were compared with ESDU, which provides generic representations of atmospheric boundary layer (ABL) profiles based on full-scale field data [5,6]. The profiles used are vertical profiles at the centre of the roughness elements (midpoint between the successive rows of roughness elements and across the wind tunnel). The log law parameters z_o and d were determined by fitting the vertical streamwise velocity profile to log law equations (Eq. 3) with u_* estimated from the vertical profile of the Reynolds shear stress in the constant stress region located just above the roughness height (Fig. 7b).

$$\overline{U}(z) = \frac{u_*}{k}\left[\ln\left(\frac{z-d}{z_o}\right)\right]$$

(3)

The integral length scales of the streamwise velocity were estimated from the temporal correlation coefficient from the PIV data and mean streamwise velocity at the corresponding height using Taylor's hypothesis of frozen turbulence (Eq. 4).

$$L_u(z) = \int R_{uu}(z, \tau)d\tau * U(z)$$

(4)

Fig. 3 Example of temporal
correlation obtained at z = 4h
from PIV (*open triangle*) and
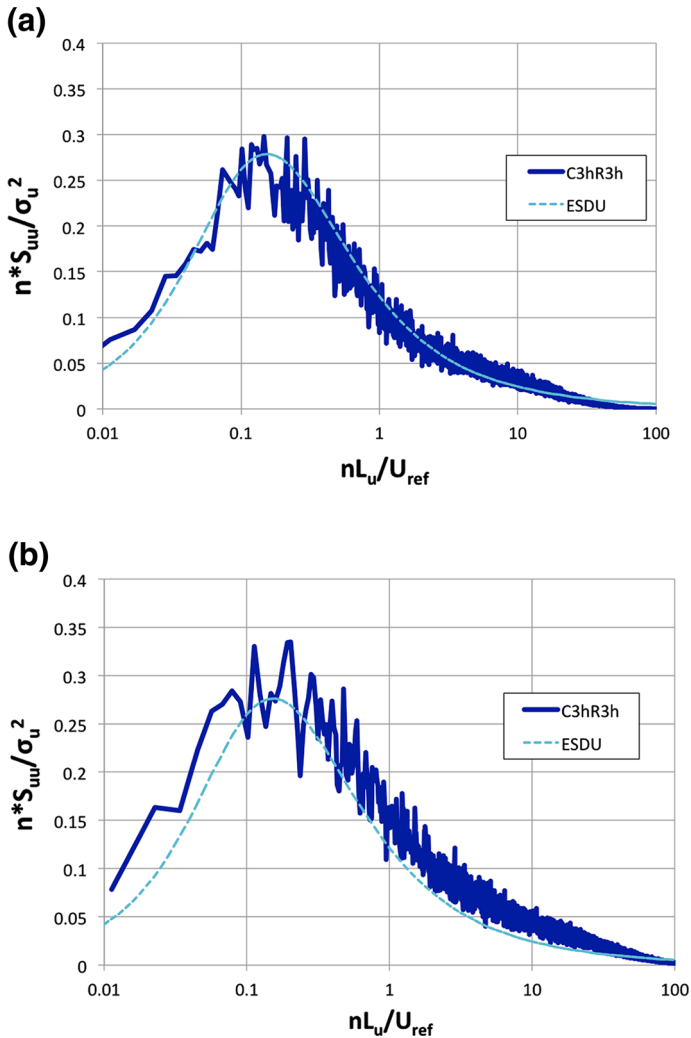HWA (*solid line*). *Solid line*
exponential fit to the PIV results
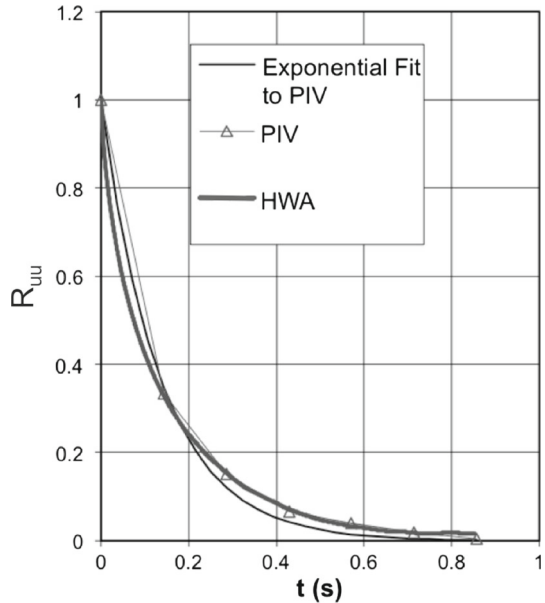
Given the low time-resolution of the PIV system (7 Hz), the integral time scale was estimated
by fitting an exponential decaying function to the temporal correlation obtained from the
PIV. To assess the validity of the method, an example of a computed temporal correlation
is shown in Fig. 3, together with the same quantity obtained from well time-resolved hot-
wire measurements and the exponential fit. The best match scale of the boundary layer
configurations are 1:100, 1:200 and 1:100 for R1h, Rcu and R3h, respectively. When using
z_o as an indicator, the terrains vary, with R1h being rural ($z_o = 0.03$ m), Rcu being between
outskirts and suburban ($z_o = 0.2$ m) and R3h being urban ($z_o = 0.7$ m). The profiles are
shown in Fig. 4 along with the corresponding ESDU profiles. The integral length scale is
not precisely modeled in the higher altitudes, which is typically the case in wind tunnel
simulations as the size of the eddies is limited by the cross-sectional dimensions of the wind
tunnel, the size of the vorticity generators at the entrance of the working section and the
thickness of the boundary layer that can be generated over the available fetch length. From a
comparison with the spectral density it is evident that the turbulence is modeled well within
the boundary layer ($z - d < 5$ h) (Fig. 5). The Jensen number, which is the ratio of z_o
to characteristic building height h, scaling results in an approximate scaling of 1:250 or a
full-scale building height of 12.5 m for all three boundary layers within an acceptable factor
of 2-3. Thus, the profile scaling with ESDU would suggest a full-scale building height of 5
m for R1h and R3h and 10 m for Rcu.

3.2 Comparison of boundary layer characteristics for different upstream roughness

The following section considers only the three upstream boundary layers studied, which are
Rcu, R1h and R3h. For the R1h and R3h cases measurements were taken above the canyon,
which is of equal AR to the roughness elements and for the Rcu case, measurements were
taken above the cube roughness.
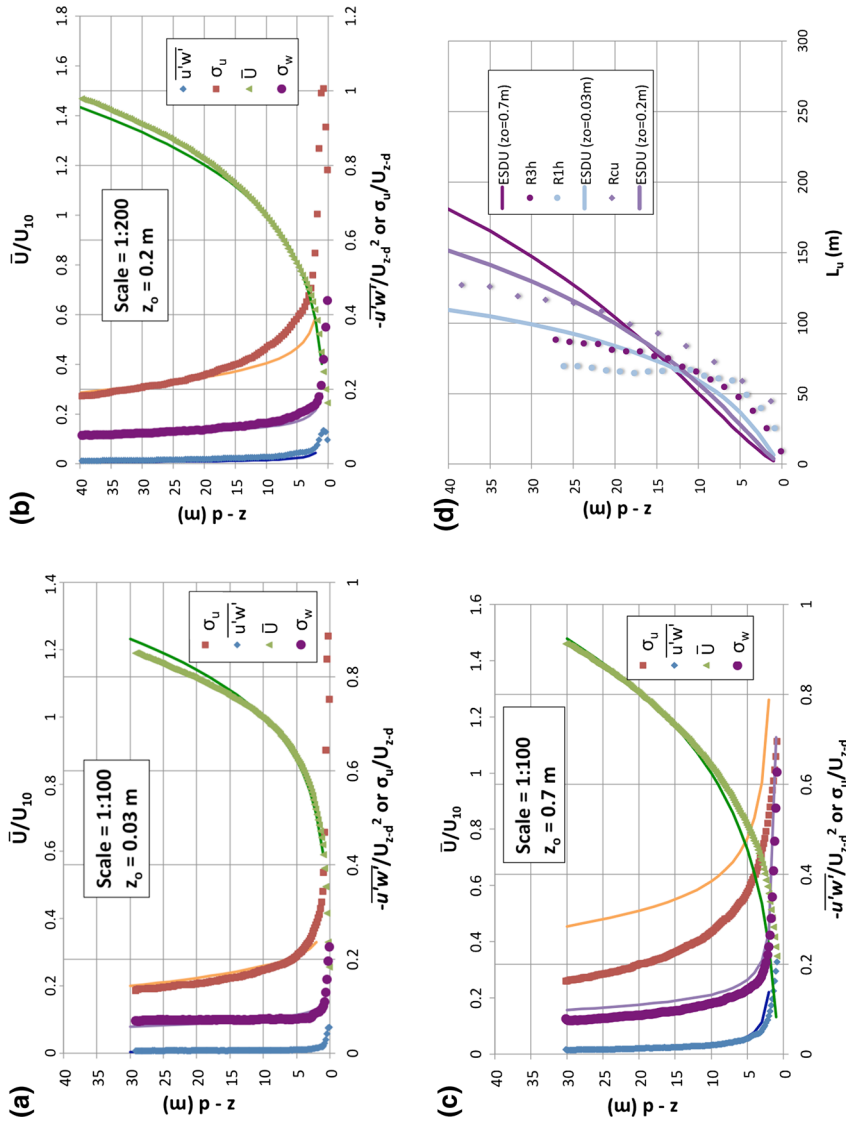
Fig. 4 Comparison between ESDU [5,6] boundary layer profiles and centre vertical PIV profiles for different scaling factors **a** R1h; **b** Rcu; **c** R3h; **d** streamwise integral length scales. *Lines* denote ESDU profiles and *points* denote experimental data

(a)

(b)

Fig. 5 Spectral denisty of the streamwise component obtained at height of **a** z = 2h and **b** z = 4h from HWA measurements (*solid line*) compared to the ESDU [5,6] model (*dashed line*) for C3hR3h

3.2.1 Boundary layer characteristics

The boundary layer characteristics provide insight into the effects of varying the roughness density and configuration. These characteristics were calculated using both the spatially averaged vertical profile across the width of the canyon and the centre vertical profile as specified in Table 3. When using the friction velocity to normalize other quantities the value used corresponds to the vertical profile, either spatially averaged or centre. When considering the spatially averaged values with increased plan area density, from Rcu and R3h to R1h, the friction velocity and roughness length decrease while the zero-plane displacement increases (Table 3). This is a result of the increased plan area density of R1h and the skimming flow regime. When comparing the centre values the same pattern is evident for the friction velocity,
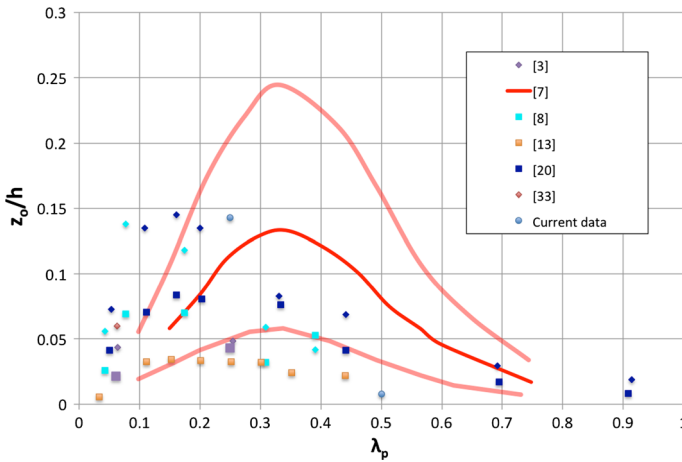
Fig. 6 Boundary layer roughness length of the present study (blue circles) compared with the review from Grimmond and Oke [7] (*dark line* mean values, *light lines* outer limits) and experimental data from the literature [3,8,13,20,33]. *Circles* 2D configurations; *squares* 3D aligned configurations; *diamonds* 3D staggered configurations

which suggests the evolution of this parameter with λ_p is not sensitive to spatial averaging. Although the roughness length exhibits the same trend there is some variability between the spatially averaged and centre profiles suggesting that this value is sensitive to spatial averaging. Finally, the centre zero-plane displacement results in significantly different values between the spatially averaged and centre values, again suggesting sensitivity to spatial averaging. Grimmond and Oke [7] modeled z_o and d as a function of λ_p. These values are shown in Fig. 6 along with the current data and other studies of different configurations including 2D, 3D aligned [8,13,20] and 3D staggered [3,33]. All of the results shown are calculated from spatially averaged vertical streamwise velocity profiles, including those values taken from the literature. It is evident that 2D roughness arrays result in higher z_o than 3D roughness arrays of equal λ_p. As well, staggered 3D arrays result in higher z_o than aligned, with this difference being greater with lower λ_p. In the present case, the R1h and R3h configurations have a plan area density of 50 and 25 %, respectively. When compared to those from the model of Grimmond and Oke [7], the roughness parameters found in the present study vary significantly. However, the cases with $\lambda_p = 25$ % lie within the outer limits provided by Grimmond and Oke [7] based on all the data they compiled, whereas the 2D $\lambda_p = 50$ % case does not lie within the outer limits provided. The discrepancy is likely to be the result of the differences in roughness configuration between the cases as can be seen when comparing 2D and 3D configurations that have the same plan area density. Thus, not only do the boundary layer parameters depend on the plan area density, but also on the geometry of the roughness elements.

3.2.2 Spatially averaged turbulence statistics

The mean statistics of the roughness boundary layers, including vertical profiles of mean streamwise velocity and Reynolds shear stress were spatially averaged across the width of the canyon and normalized by the freestream velocity to give a representative profile for each boundary layer studied. The mean velocity profiles (Fig. 7a) show that in the skim-
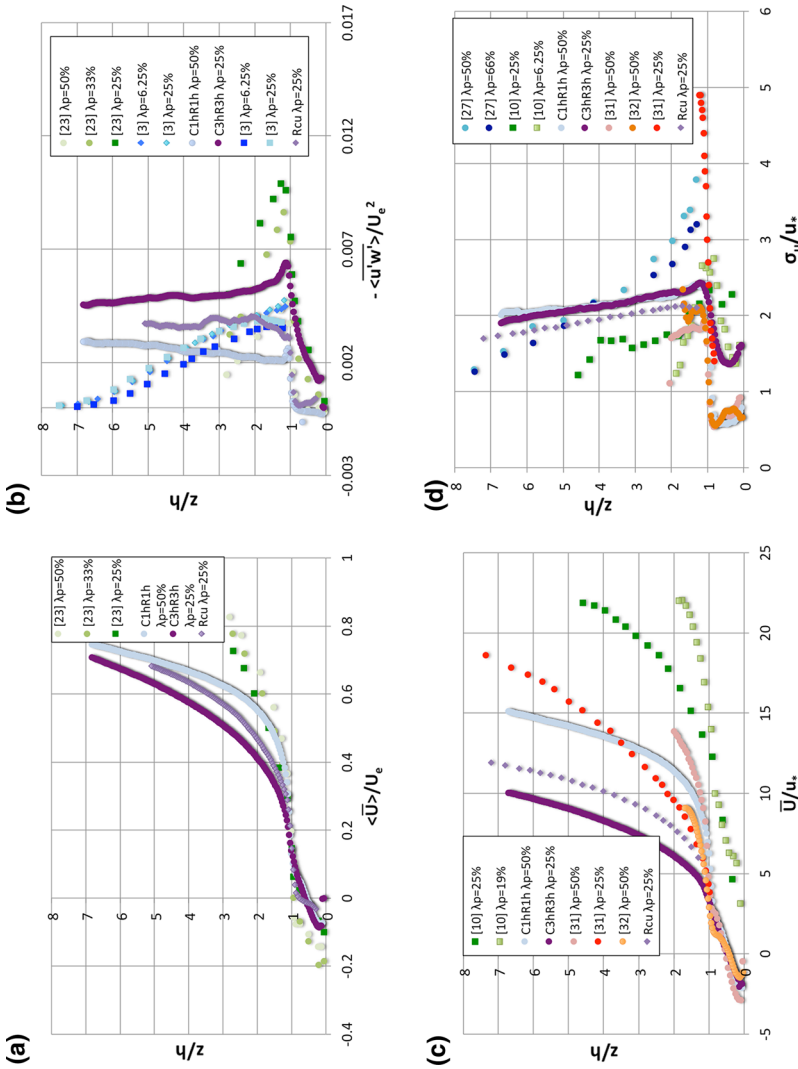
Fig. 7 Comparison of approaching boundary layer flow statistics from the present study with results from literature for **a** spatially averaged mean streamwise velocity [23]; **b** spatially averaged shear stress [3,23] **c** centre mean streamwise velocity [10,31,32]; **d** centre turbulence intensity [10,27,31,32]. Spatially averaged quantities are normalized by freestream velocity and centre quantities are normalized by friction velocity derived from centre profiles. *Circles* 2D configurations; *squares* 3D aligned configurations; *diamonds* 3D staggered configurations

ming flow regime case (R1h) the mean velocity is larger than that of R3h, which is in the wake interference regime. With equal λ_p the 3D configuration results in larger streamwise velocity than the 2D configuration, which is likely a result of obstacle spacing making the 3D configuration a skimming flow. The results of Michioka and Sato [23] do not show a significant trend between cases, which may be a result of all of their configurations laying within the skimming flow regime. From the earlier review, there is no significant difference in the mean velocity profiles between aligned and staggered 3D arrays [19]. As well, the magnitude of the velocity depends on λ_p for 2D cases [13,31] and the current results confirm this observation. The spatially averaged shear stress shows the opposite trend with the higher AR having a larger shear stress, which is confirmed by the results of Michioka and Sato [23] (Fig. 7b). Salizzoni et al. [31] also confirm this pattern, but Marciotto and Fisch [22] found that the shear stress is not dependent on λ_p. 3D configurations of aligned and staggered arrays show, that in both cases, an increase in λ_p results in an increase in the shear stress [3]. When comparing the current study's 3D configuration with the 2D configuration of equal λ_p the 3D configuration results in lower magnitudes of shear stress. This suggests that the 3D configuration is within the skimming flow regime. This is confirmed by Michioka and Sato [23] who found that with equal AR the shear stress increases from 2D to 3D, but contradicted by Lee et al. [16] and Volino et al. [35] who found the opposite to be true. This contradiction may be attributed to the flow regime. Within the skimming flow regime 3D configurations have a larger magnitude of shear stress than 2D configurations, but within the wake interference regime 3D configurations have smaller magnitudes of shear stress than 2D configurations.

3.2.3 Centre turbulence statistics

The centre vertical profiles of the mean streamwise velocity and streamwise turbulence intensity are normalized by the friction velocity derived from the centre vertical profiles (Fig. 7c, d). The centre mean velocity profiles follow the same pattern as the spatially averaged profiles with an increase in AR resulting in decreased velocity [23]. There is a significant difference between the results of the current study and those of Salizzoni et al. [31] and Sato et al. [32] for 2D configurations of equal AR. 3D arrays were found to have the opposite pattern to 2D arrays with the larger AR resulting in larger velocities [10]. The streamwise turbulence intensity (σ_u) above the roughness array is similar for both 2D configurations of the current study where σ_u is governed by the boundary layer simulation conditions, but within the roughness array the wake interference regime case has larger σ_u. This suggests that in the skimming flow regime there is less turbulence produced in the lower part of the boundary layer. Turbulence is generated from the mean shear. Skimming flow produces less mean shear at the downstream canyon obstacle where flow impinges at the top of the wall, whereas wake interference has strong separation and, hence, stronger mean velocity gradients at the leading corner of the downstream canyon obstacle. The apparent similarity of the streamwise turbulence intensity above the canyon between the two 2D configurations of the present work is contradicted by Salizzoni et al. [31] and Huq and Franzese [10] who determined that σ_u increases with increasing AR. Furthermore, it contradicts the observations made in previous studies which found that σ_u is suppressed in the skimming flow regime, resulting in higher magnitudes above the roughness array in the wake interference regime [9,18,31]. However, the 3D configuration results in slightly lower σ_u magnitudes above the roughness array. When compared with other studies of the same configurations there is some discrepancy [27,31,32]. The differences between skimming flow regime cases are less than the wake interference cases as skimming flow is less sensitive to boundary layer conditions.

3.2.4 Turbulent kinetic energy

The TKE and the relative contribution of each orthogonal component is analyzed for the three upstream roughness configurations (Fig. 8). The streamwise component of velocity contributes most to the total TKE with the vertical component contributing the least. A field experiment conducted in Zurich, Switzerland, supports this result [30]. Figure 8d shows the relative contribution of each velocity component to the total TKE within the roughness ($z/h = 0.5$), within the shear layer ($z/h = 1$) and above the shear layer ($z/h = 3$). The proportion of the streamwise velocity component is highest within the shear layer and in the overlying boundary layer. However, within the roughness the contribution of the spanwise and vertical components are increased and the streamwise contribution is decreased. The large magnitudes of relative contribution within the roughness are a result of low magnitudes of total TKE present within the roughness. The results also show that an increase in λ_p results in decreased variance of the streamwise velocity component, but increased variance of the spanwise and vertical velocity component, specifically within the roughness and in the outer region. The effect of array obstacle configuration is also apparent within the shear layer as the 3D Rcu case results in decreased variance of the streamwise and spanwise velocity component and increased variance of the vertical velocity component compared to the 2D case of equal λ_p. These results demonstrate that 2D and 3D configurations of equal λ_p do not result in similar relative contribution to total TKE profiles. When compared to the results of Macdonald and Carter Schofield [21] for an aligned 3D array with $\lambda_p = 25$ % the current results have larger magnitudes for the streamwise turbulence intensity for all configurations. The results correspond well to the R3h case for the vertical component to a height of approximately $z/h = 4$, but then begin to decrease [21]. The spanwise contribution is higher than the current results by a significant amount. It is apparent that the contribution of each velocity component to the total TKE of aligned and staggered cube arrays is not the same.

3.2.5 Streamwise integral length scale

The influence of the geometry of the upstream roughness elements is also assessed via the estimation of the streamwise integral length scale (L_u), which is an important parameter when classifying boundary layers and is calculated as outlined in Sect. 3.1. In the region just above the roughness to a height of approximately 3 h, the length scales for R3h and R1h are similar, while in the Rcu case the scales are smaller (Fig. 9). At heights above 3h the length scales of the Rcu are again the smallest, but there is some deviation between the R3h and R1h cases with the lower AR configuration having smaller length scales. This deviation is likely to be due to the different growth rates of the internal boundary layers that develop after the change of roughness geometry, the rougher the surface, the faster the growth (Fig. 2). Nevertheless, the present results agree with those of Volino et al. [35] who found that the length scales of the 2D roughness case were significantly higher than the 3D case throughout the height of the boundary layer. Conversely, the present results and those of Volino et al. [35] are contradicted by Takimoto et al. [34] whose results show that 3D configurations result in larger L_u than those of 2D configurations with equal AR. This discrepancy may be a result of the simulation method leading to a smaller boundary layer to building height ratio as no spires were used by Takimoto et al. [34] to produce turbulence and it is clear that L_u tapers off to very small values with increasing height in their work. All results seem to approach a similar value as z/h approaches unity except the 2D configuration of Volino et al. [35] with a high AR.
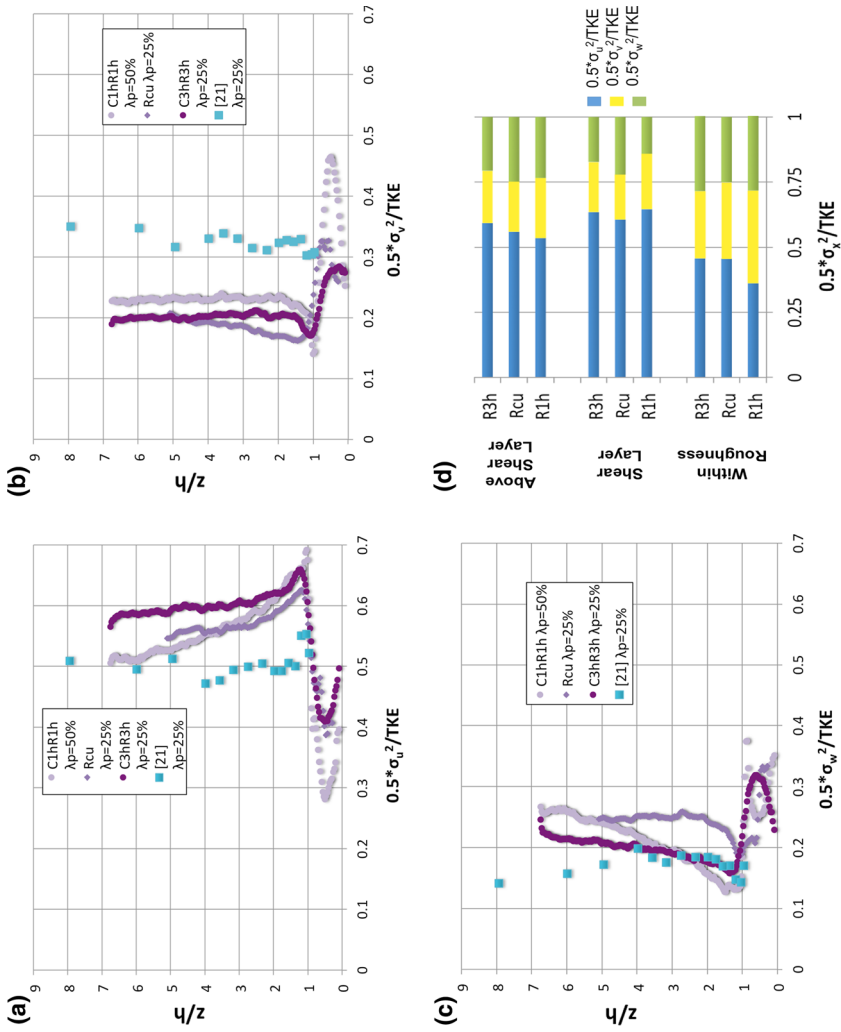
Fig. 8 Comparison of contribution to total TKE of **a** streamwise velocity component; **b** spanwise velocity component; **c** vertical velocity component with literature [21]; **d** proportion of each TKE component at different heights. *Circles* 2D configurations; *squares* 3D aligned configurations; *diamonds* 3D staggered configurations
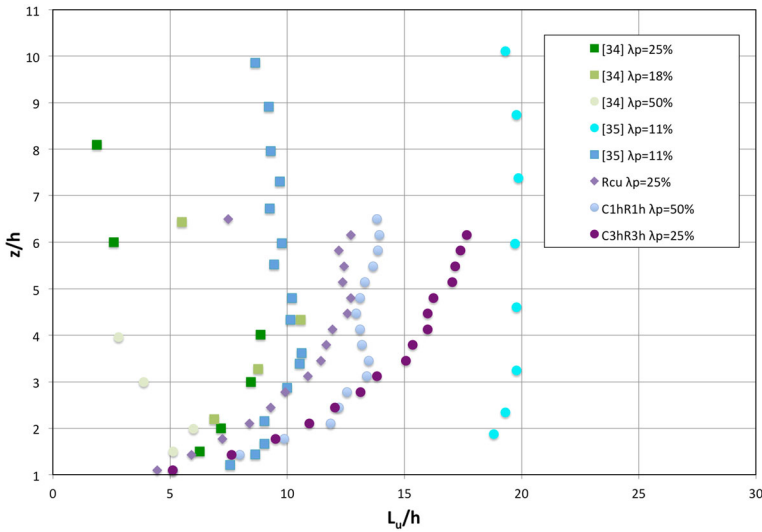
Fig. 9 Streamwise integral length scales compared with data from literature [34,35]. *Circles* 2D configurations; *squares* 3D aligned configurations; *diamonds* 3D staggered configurations

3.3 Comparison of canyon flow regimes

Previous work attempting to classify the canyon dynamics of varying upstream roughness spacing are compared to the present work, normalized by the friction velocity derived from the centre vertical shear stress profiles (Fig. 10). These profiles are measured with the 2D test canyon for all three upstream roughness configurations. When comparing the mean streamwise velocity centre profiles there is no significant difference between the canyons of AR = 1 and 3 (C1h and C3h) configurations for each respective upstream roughness. The differences between canyon configurations is not significant above the shear layer in the σ_u centre profiles. However, the σ_u peaks are larger for all C3h compared to C1h configurations within the shear layer. This suggests that the size of the measurement canyon has little impact on the turbulent statistics above the canyon, which are mostly influenced by the upstream roughness configuration, but does have a significant impact on the shear layer.

The vorticity thickness (δ_w) of a mixing layer is a measure of the vertical extent of the shear layer over the canyon. It was calculated by determining the maximum velocity gradient over the canyon opening using the finite difference method and the velocity difference, which was selected to be between the free streamwise velocity and zero at the bottom of the canyon (Eq. 5). The location of the maximum gradient was recorded and the location and boundaries of the shear layer were determined by adding and subtracting half of the vorticity thickness from the location of the maximum gradient.

$$\delta_w = \frac{\Delta U}{(dU/dy)_{max}} \tag{5}$$

Comparing the shear layers of the different configurations shows that the C3h results in much wider shear layers than C1h with greater penetration into the canyon (Fig. 11a, b). It is evident in both the C1h and C3h cases that the upstream roughness changes the shape and size of the shear layer. Rcu and R3h result in similarly sized and shaped shear layers, whereas the R1h results in slightly smaller shear layers in both canyon configurations. This
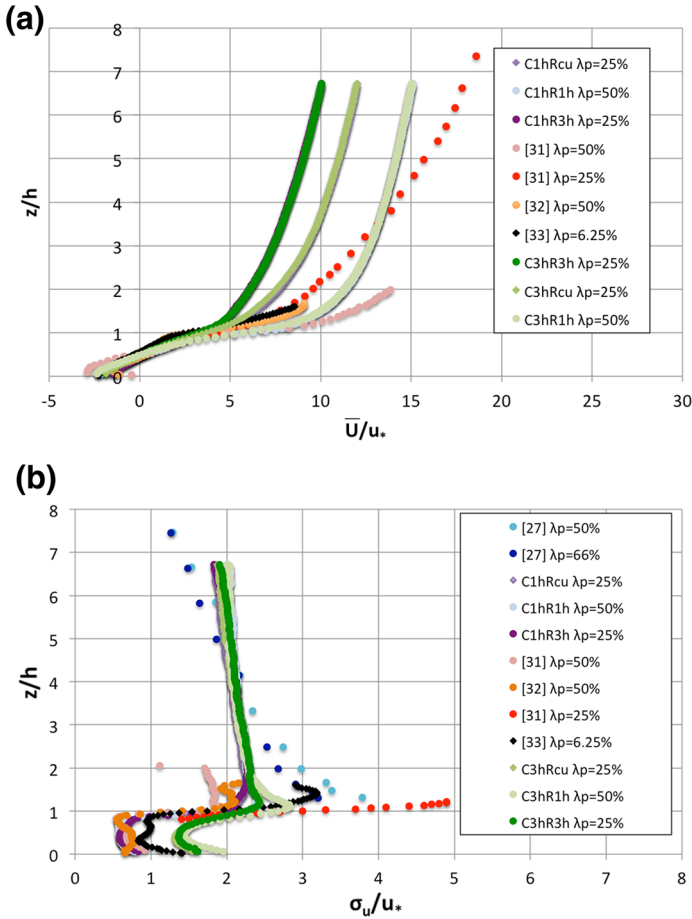
Fig. 10 **a** Centre streamwise mean velocity measured within the canyon normalized by friction velocity derived from centre profiles compared with literature [31–33]; **b** turbulence intensity normalized by friction velocity derived from centre profiles measured within the canyon compared with literature [27,31–33]. *Circles* 2D configurations; *squares* 3D aligned configurations; *diamonds* 3D staggered configurations

is interesting to note as both R3h and Rcu have the same plan area density (25 %), which may explain the similarity.

The shear layer TKE production can also be used to determine the shear layer boundaries (Eq. 6). The gradient of the TKE production is then used to define the boundaries with a threshold value. This threshold value is not given by Salizzoni et al. [31] and was determined in the present case as the value at the base of the peak in the TKE production gradient.

$$P = \overline{u'u'}\frac{\partial \overline{u}}{\partial x} + \overline{u'w'}\frac{\partial \overline{u}}{\partial z} + \overline{w'u'}\frac{\partial \overline{w}}{\partial x} + \overline{w'w'}\frac{\partial \overline{w}}{\partial z} \tag{6}$$

This method is used with the current results for comparison purposes (Fig. 12). From the comparison it is evident that the shear layers of all three configurations are similar with only a slightly higher boundary in the C1hR3h configuration. The configurations of Salizzoni et al. [31] result in lower and thinner shear layers, which agrees with the larger peak in the
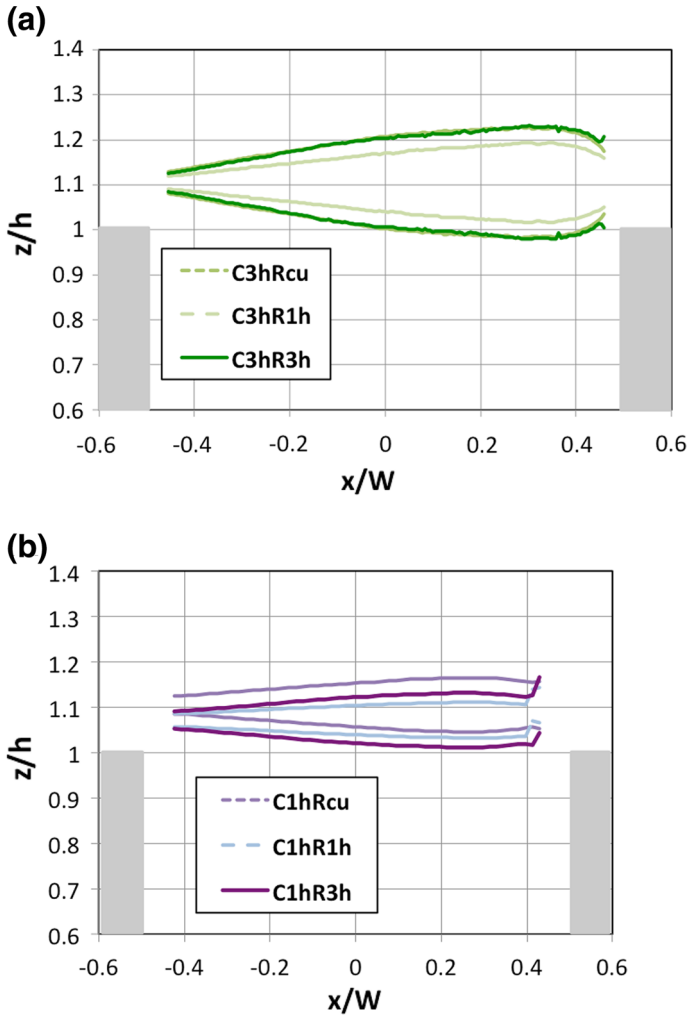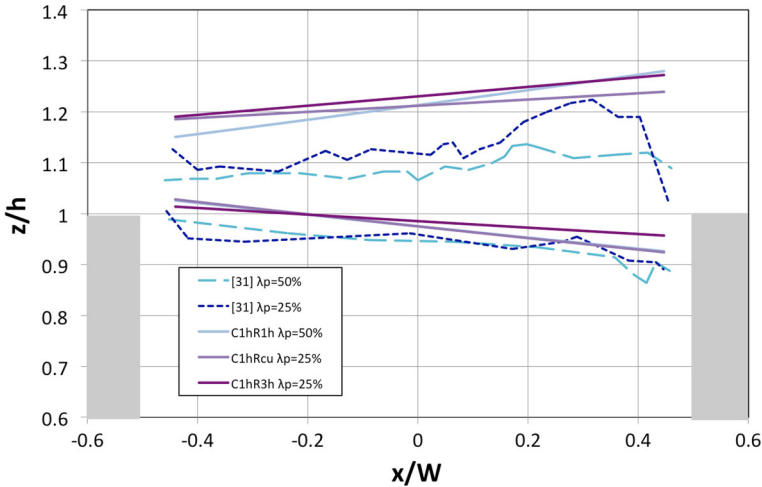
Fig. 11 Shear layer boundaries of **a** the C3h and **b** C1h canyon configurations for the 3 different types of approaching flows. *Dotted* 3D cubes; *dashed* 2D bars AR = 1; *solid* 2D bars AR = 3

turbulence intensity profiles shown previously. This may be a result of differences in the height of turbulence generators used as the present study used generators of approximately 16h compared to 8h used by Salizzoni et al. [31].

In order to further quantify the effect of the upstream roughness configuration on the canyon flow, the time-averaged vertical flow rate across the canyon opening was computed as:

$$Q = \frac{L}{N} \sum_{j=1}^{N} \int_{x=-W/2}^{x=W/2} w(z = h, t_j) dx \qquad (7)$$

where w is the instantaneous vertical velocity, W is the canyon width, L is the canyon lateral length and N is the number of PIV images used for averaging. The computation

Fig. 12 Shear layer boundaries of C1h canyon configurations for the 3 different types of approaching flows using TKE Production method compared with [31]

was performed at the centre of the canyon (y = 0). The total flow rate Q was decomposed into its positive (upward) and negative (downward) contributions. Using $w = W + w'$, the contribution of both the mean (W) and the fluctuating (w') velocities to the flow rate was estimated. Given the high aspect ratio L/h of the investigated canyons, one could expect the flow to be statistically homogeneous in the transverse direction. The combination of this hypothesis with the configuration of the canyon axis perpendicular to the main flow leads to a zero contribution of the mean flow to the total flow rate at the canyon opening. The results presented in Fig. 13a show a small positive contribution of the mean flow to the total flow rate (x). These values correspond to mean vertical velocities of the order of magnitude of the statistical error (Sect. 2). The possibilities of the canyon being slightly off with its theoretical axis or of a slight misalignment of the measurement plane with the main flow were investigated by estimating the mean transversal flow rate needed to compensate the non-zero vertical flow rate. It was found to correspond to angular offset lower that 0.7°, a value smaller than the accuracy that can be achieved in setting up such experiment. The non-zero values of the mean total rate are, therefore, considered to have no statistical significance. Mass transfer between the canyon and the boundary layer should, therefore, be considered as being caused by turbulent fluctuations.

The results are shown in Fig. 13a. For both canyon AR studied, changing from a skimming to a wake interference flow regime in the upstream roughness (and in agreement with the shear layer analysis) increases the magnitude of the total positive and negative flow rates (filled triangles), which is due to an increase of the contribution of the fluctuating velocity. When comparing the present configurations with equal λ_p the 2D configuration has a higher flow rate than the 3D case. This is due to the transition from skimming flow in the 3D case to wake interference flow in the 2D case. The results are compared to those of Ho and Liu [9] (Fig. 13b) and it is evident that the current configurations result in lower magnitudes for the total flow rate and the turbulent flow rate. It is apparent that for all configurations the majority of the instantaneous flow rate across the canyon is due to the turbulence fluctuations.

(a)

(b)
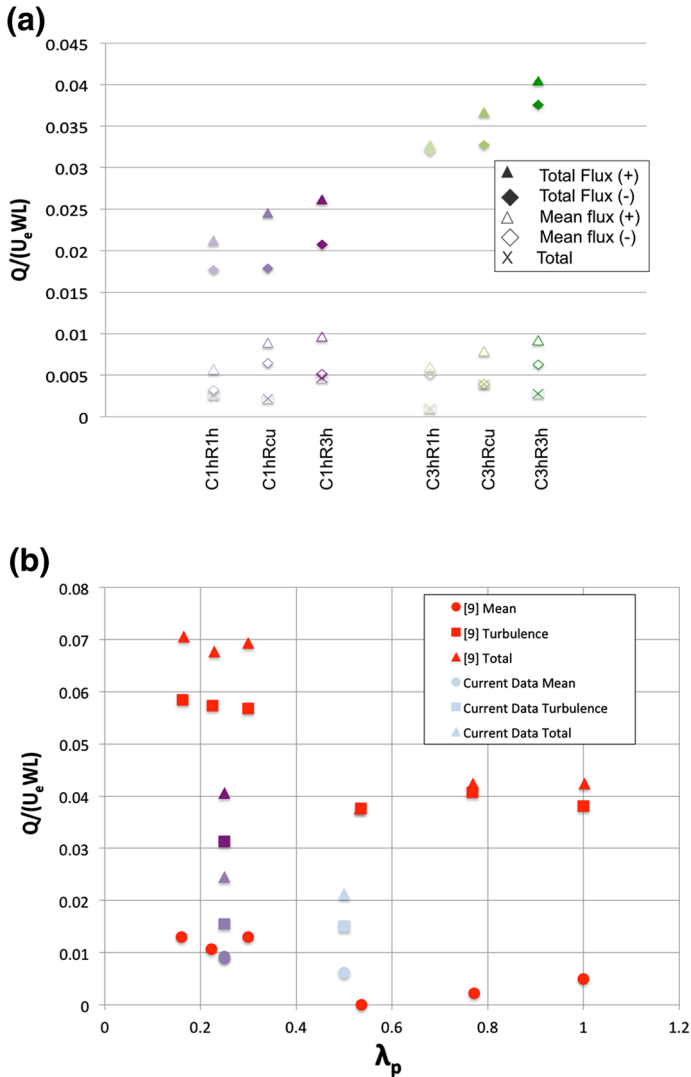
Fig. 13 **a** Positive flow rate across the canyon (*filled triangle*), negative flow rate across the canyon (*filled diamond*) and total flow rate across the canyon (×) flow rate, $Q/U_e WL$, across the canyon for the 6 different configurations (*W* canyon streamwise width, *L* canyon lateral length); *open symbols* contribution of the mean flow to the flow rate; *filled symbols* contribution of both the mean flow and fluctuation to the flow rate; **b** Air Exchange Rate (ACH) of present results (*open symbols*) compared with [9] (*filled symbols*) with contribution from mean (*circles*), turbulence (*squares*) and total (*triangles*) for three configurations

4 Conclusions

The geometry of the roughness elements (cubes or 2D bars with different streamwise spacing) in the upstream roughness used to simulate an atmospheric boundary layer was found to have a non-negligible influence on the characteristics of the boundary layer. The effect of roughness plan area density (λ_p) is evident within the vertical profiles of mean streamwise

velocity, shear stress, turbulence intensity and integral length scales. The current results agree with previous work, which found that the mean streamwise velocity for configurations of equal λ_p is higher in the 3D than 2D configuration [10,31]. The relative contribution of the three orthogonal components to the total turbulent kinetic energy (TKE) also agrees with published data and demonstrates that staggered and aligned arrays or 2D and 3D arrays of equal λ_p do not generate the same profiles of TKE [21,30]. The current results show that the integral length scale is larger in 2D than 3D cases of equal λ_p and confirms that the integral length scale also increases with increasing AR in 2D configurations [35]. The spatially averaged turbulent shear stress increases with decreasing λ_p for 2D configurations, as confirmed by the literature [23]. The spatially averaged shear stress is also shown to increase from the 3D to 2D configuration of equal λ_p, in contradiction to previous work [23]. The current results show that the canyon ventilation flow rate increases from 3D to 2D configurations of equal λ_p and increases with decreasing λ_p. This is due to the transition from skimming to wake interference regimes. Comparing the roughness length (z_o) for 2D and 3D configurations of equal λ_p shows that 2D configurations result in larger magnitudes. ESDU scaling was used to classify the three upstream roughness configurations. The scaling suggests that the R1h configuration represents a scenario that is not applicable to the study of street canyon ventilation and, thus, this configuration should not be used in further studies wishing to investigate urban street canyon flows. This is confirmed by the very high value of the displacement height (d/h > 0.98), which is not compatible with the estimated nature of the terrain (rural).

The influence of the different approach flows on the flow inside a street canyon model was investigated for two different canyon streamwise widths (W). An increase in canyon width resulted in higher turbulence intensity peaks within the shear layer and increased vertical canyon ventilation rate. However, there is a negligible effect on the streamwise velocity and turbulence intensity above the canyon, which suggests that these parameters and the outer flow are mostly influenced by the upstream roughness. The increased canyon width resulted in a larger shear layer with all upstream roughness configurations and it is also evident that the 2D R1h (square section obstacles spaced at 1 h) configuration results in a slightly smaller shear layer with both measurement canyon configurations. The ventilation of the canyon, estimated via the computation of positive and negative flow rate across the canyon opening, was found to be influenced by the upstream flow regime, even with a canyon with W/h = 1. An upstream wake-interference flow regime leads to stronger exchanges between the canyon and the flow above by enhancing both the turbulence and the mean flow contribution to the flow rate. Thus, it is evident that care must be taken when selecting the upstream roughness element configuration for a given wind tunnel study, depending on which regime (wake interference or skimming) is desired for the oncoming flow and, separately, for the test canyon.

References

1. Barlow JF, Leitl B (2007) Effect of roof shapes on unsteady flow dynamics in street canyons. In: International Workshop on Physical Modelling of Flow and Dispersion Phenomena (PHYSMOD) August 2007, Orléans

2. Chang K, Constantinescu G, Park S (2006) Analysis of the flow and mass transfer processes for the incompressible flow past an open cavity with a laminar and a fully turbulent incoming boundary layer. J Fluid Mech 561:113–145
3. Cheng H, Hayden P, Robins AG, Castro IP (2007) Flow over cube arrays of different packing densities. J Wind Eng Ind Aerodyn 95:715–740
4. Coceal O, Dobre A, Thomas TG, Belcher SE (2007) Structure of turbulent flow over regular arrays of cubical roughness. J Fluid Mech 589:375–409
5. ESDU (1982) Strong winds in the atmospheric boundary layer. Part I: mean-hourly wind speeds. Data Item 82026 (amended 1993), Engineering Sciences Data Unit International
6. ESDU (1985) Characteristics of atmospheric turbulence near the ground. Part II: single point data for strong winds (neutral atmosphere. Data Item 852020 (amended 1993), Engineering Sciences Data Unit International
7. Grimmond CSB, Oke TR (1999) Aerodynamic properties of urban areas derived from analysis of surface form. J Appl Meteorol 38:1262–1292
8. Hagishima A, Tanimoto J, Nagayama K, Meno S (2009) Aerodynamic parameters of regular arrays of rectangular blocks with various geometries. Bound Layer Meteorol 132:315–337
9. Ho YK, Liu CH (2013) Wind tunnel modeling of flows over various urban-like surfaces using idealized roughness elements. In: International Workshop on Physical Modelling of Flow and Dispersion Phenomena (PHYSMOD) Sept 2013, University of Surrey
10. Huq P, Franzese P (2013) Measurements of turbulence and dispersion in three idealized urban canopies with different aspect ratios and comparisons with Gaussian plume model. Bound Layer Meteorol 147: 103–121
11. Jensen NO (1978) Change of surface roughness and the planetary boundary layer. Quart J R Meteorol Soc 104:351–356
12. Kaimal JC, Finnigan JJ (1994) Atmospheric boundary layer flows: their structure and measurement. Oxford University Press, Oxford
13. Kanda M, Moriwaki R, Kasamatsu F (2004) Large-eddy simulation of turbulent organized structures within and above explicitly resolved cube arrays. Bound Layer Meteorol 112:343–368
14. Kanda M (2006) Large-eddy simulations on the effects of surface geometry of building arrays on turbulent organized structures. Bound Layer Meteorol 118:151–168
15. Kang W, Sung HJ (2009) Large-scale structures of turbulent flows over an open cavity. J Fluids Struct 25:1318–1333
16. Lee JH, Sung HJ, Krogstad P (2011) Direct numerical simulation of the turbulent boundary layer over cube-roughened wall. J Fluid Mech 669:397–431
17. Lee JH, Seena A, Lee SH, Sung HJ (2012) Turbulent boundary layers over rod- and cube-roughened walls. J Turb 13:1–26
18. Liu CH, Leung DYC, Barth MC (2005) On the prediction of air and pollutant exchange rates in street canyons of different aspect ratios using large-eddy simulation. Atmos Environ 39:1567–1574
19. Macdonald RW (2000) Modelling the mean velocity profile in the urban canopy layer. Bound Layer Meteorol 97:23–45
20. Macdonald RW, Griffiths RF, Hall DJ (1998) An improved method for the estimation of surface roughness of obstacle arrays. Atmos Environ 32:1857–1864
21. Macdonald RW, Carter Schofield S (2002) Physical modelling of urban roughness using arrays of regular roughness elements. Water Air Soil Pollut 2:541–554
22. Marciotto ER, Fisch G (2013) Wind tunnel study of turbulent flow past an urban canyon model. Environ Fluid Mech 13:403–416
23. Michioka T, Sato A (2012) Effect of incoming turbulent structure on pollutant removal from two-dimensional street canyon. Bound Layer Meteorol 145:469–484
24. Oke TR (1988) The urban energy balance. Prog Phys Geogr 12:471–508
25. Panofsky HA, Dutton JA (1984) Atmospheric turbulence: models and methods for engineering applications. Wiley, New York
26. Perret L, Savory E (2013) Large-scale structures over a single street canyon immersed in an urban-type boundary layer. Bound Layer Meteorol 148:111–131
27. Rafailidis S (1997) Influence of building areal density and roof shape on the wind characteristics above a town. Bound Layer Meteorol 85:255–271
28. Ricciardelli F, Polimeno S (2006) Some characteristics of the wind flow in the lower urban boundary layer. J Wind Eng Ind Aerodyn 94:815–832
29. Rivet C (2014) Étude en soufflerie atmosphérique des interactions entre canopée urbaine et basse atmosphère par PIV stéréoscopique. Dissertation, École Centrale de Nantes

30. Rotach MW (1995) Profiles of turbulence statistics in and above an urban street canyon. Atmos Environ 29:1473–1486
31. Salizzoni P, Marro M, Soulhac L, Grosjean N, Perkins R (2011) Turbulent transfer between street canyons and the overlying atmospheric boundary layer. Bound Layer Meteorol 141:393–414
32. Sato A, Takimoto H, Michioka T (2009) Impact of wall heating on air flow in urban street canyons. In: International Workshop on Physical Modelling of Flow and Dispersion Phenomena (PHYSMOD) August 2009, Brussels
33. Savory E, Perret L, Rivet C (2013) Modelling considerations for examining the mean and unsteady flow in a simple urban-type street canyon. Meteorol Atmos Phys 121:1–16
34. Takimoto H, Inagaki A, Kanda M, Sato A, Michioka T (2013) Length-scale similarity of turbulent organized structures over surfaces with different roughness types. Bound Layer Meteorol 147:217–236
35. Volino RJ, Schultz MP, Flack KA (2009) Turbulence structure in a boundary layer with two-dimensional roughness. J Fluid Mech 635:75–101